World Electric Vehicle Journal

MDPI

Article

Comparative Analysis of MacPherson and Double Wishbone Suspensions for an Electric Off-Road Vehicle Retrofit

Pablo Tapia [1], Eugenio Tramacere [2], David Sebastian Puma-Benavides [3,4,*], Renato Galluzzi [1,*], Victor Danilo Zambrano-Leon [5], Juan Carlos Jima-Matailo [6] and Edilberto Antonio Llanes-Cedeño [4,*]

1 School of Engineering and Sciences, Tecnologico de Monterrey, Mexico City 14380, Mexico; a01769991@tec.mx
2 Center for Automotive Research and Sustainable Mobility (CARS), Politecnico di Torino, 10129 Turin, Italy; eugenio.tramacere@polito.it
3 School of Engineering and Sciences, Tecnologico de Monterrey, Puebla 72453, Mexico
4 Department of Mechanics, Universidad Internacional SEK, Quito 170503, Ecuador
5 Department of Energy Sciences and Mechanics, Universidad de las Fuerzas Armadas ESPE, Belisario Quevedo, Latacunga 050101, Ecuador; vdzambrano@espe.edu.ec
6 Automotive Mechanics, Instituto Superior Tecnologico Loja, Loja 110150, Ecuador; jcjima@tecnologicoloja.edu.ec
* Correspondence: sebastian.puma@tec.mx or david.puma@uisek.edu.ec (D.S.P.-B.); renato.galluzzi@tec.mx (R.G.); antonio.llanes@uisek.edu.ec (E.A.L.-C.)

Abstract: The suspension system in plays a pivotal role, especially in off-road vehicles, in ensuring optimal comfort, road holding and ride safety. This study explores the transition from a MacPherson strut to a double wishbone suspension system, emphasizing its impact on relevant suspension features, such as camber and caster angles, motion ratio and vertical dynamics. Through this study, an off-road vehicle was retrofitted with the proposed suspension architecture and tested both numerically and experimentally. Test results reproduce simulation outcomes, thus confirming the effectiveness of the redesigned suspension system for the target vehicle, especially for demanding off-road applications.

Keywords: vehicle suspension; electric vehicles; MacPherson; double wishbone; vehicle retrofit

Academic Editors: Joeri Van Mierlo and Peter Van den Bossche

Received: 23 March 2025
Revised: 3 April 2025
Accepted: 11 April 2025
Published: 14 April 2025

Citation: Tapia, P.; Tramacere, E.; Puma-Benavides, D.S.; Galluzzi, R.; Zambrano-Leon, V.D.; Jima-Matailo, J.C.; Llanes-Cedeño, E.A.. Comparative Analysis of MacPherson and Double Wishbone Suspensions for an Electric Off-Road Vehicle Retrofit. *World Electr. Veh. J.* **2025**, *16*, 228. https://doi.org/10.3390/wevj16040228

1. Introduction

Automobile electrification is an ongoing trend that is gaining momentum and support throughout the world; however, its pace and depth vary significantly between regions. Although electric vehicles (EVs) are becoming a common sight in many developed countries, in developing nations the transition to EVs remains in its early stages. For example, in Ecuador and Mexico, according to AEADE and AMIA less than 5% of the new vehicles sold in 2022 were EVs [1,2]. This situation is mirrored in many countries with similar characteristics, where fleet electrification is still emerging.

This limited market penetration, driven by high costs, widespread consumer skepticism, and the perception that electric vehicles may be too delicate to withstand rough and poorly maintained roads. This contributes to the interest in and conversion of traditional internal combustion engine (ICE) vehicles into EVs. Such conversions are not entirely new; historically, gasoline-powered vehicles were often adapted to run on liquefied petroleum gas to achieve cost and emission benefits [3]. However, the current shift from an ICE to a fully electric powertrain represents a substantially more complex transformation [4], demanding a complete reevaluation of several vehicle subsystems, including the suspension.

Generally speaking, converting ICE vehicles to EVs involves replacing the engine and fuel tank with electric motors and battery packs, respectively [5]. This conversion will necessary add batteries and electric components in areas not originally designed for such elements. This can influence vehicle safety, road holding, and comfort, making it necessary to analyze the performance of the suspension system [6]. These changes affect the mass distribution, the overall weight and the center of gravity [7].

Recent literature has revealed contrasting views on suspension design for electric vehicles. Some studies emphasize the superior camber control and handling offered by double wishbone systems [8]. Beyond motorsports, these systems are essential in agricultural applications, as demonstrated by Uberti's analysis of their integration into tractor kinematics [9]. Other works advocate for simplicity and spatial efficiency through MacPherson suspensions [10]. This divergence underscores the need for a comparative analysis that not only considers performance metrics such as ride comfort and road holding, but also evaluates kinematic behavior under different driving conditions [11,12].

In parallel, suspension technology is evolving on a global scale. As EVs become more integrated with advanced control systems [13], future adaptations can involve not only adjusting conventional parameters such as camber or toe angles [14,15], but also incorporating autonomous driving functions and regenerative suspension technologies [16]. Understanding fundamental suspension kinematics in these emerging electric vehicle applications ensures the effective implementation of these mechatronic technologies, even in markets where electrification is just beginning to gain relevance.

In this context, this work aims to explore how the conversion into an EV from an ICE-powered off-road vehicle, a Suzuki Vitara, affects suspension performance, particularly in the context of its intended use. The Vitara originally features a MacPherson front suspension. This architecture is widely adopted for its simplicity and space efficiency. The rear axle of the Vitara is equipped with a torsion beam suspension. Here, we propose replacing the MacPherson system with a double wishbone suspension that is specifically designed and integrated for this vehicle model. This configuration not only provides consistent camber control and similar road holding characteristics, but also ensures that even on extremely rough terrain (comparable to an ISO 8608 D-class road [17]) the system remains usable. In addition, a key objective of this study is to ensure that if the electric battery is installed on the vehicle floor, there is sufficient clearance to absorb road irregularities without compromising safety.

This article is organized as follows. Section 1 introduces the context and background of the study. Section 2 details the methodology, describing both the original suspension and the proposed design, and highlights key differences regarding kinematic and vertical dynamics. Section 3 presents a physical implementation of the proposed solution and discusses the experimental results obtained from road tests. Finally, Section 4 concludes with recommendations for future research and potential applications in the automotive industry.

2. Method

The baseline vehicle selected for this study is the 2011 Suzuki Vitara a model introduced in Asia and South America and marketed in North America under the Chevrolet Tracker name. This vehicle has earned a strong reputation for its durability and reliability in developing regions. Direct access to this vehicle allows for precise measurements of the chassis and suspension components. In addition, official service manuals and technical diagrams were consulted to verify critical dimensions, ensuring an accurate geometric representation of the factory-installed suspension system [18]. Figure 1 and Table 1 show the baseline dimensions of the vehicle. These values are needed to better understand how the proposed suspension redesign would impact the original geometry of the vehicle.

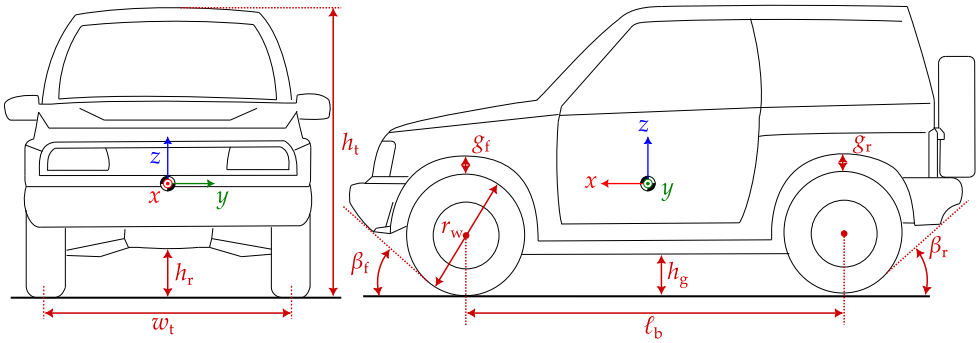

Figure 1. Baseline 2011 Suzuki Vitara geometry with key reference dimensions. Values are reported in Table 1.

Table 1. Main dimensions of the 2011 Suzuki Vitara.

Description	Symbol	Value	Unit
Track width	w_t	1395	mm
Ride height	h_r	220	mm
Overall height	h_t	1665	mm
Wheelbase	ℓ_b	2200	mm
Ground clearance	h_g	240	mm
Front fender gap	g_f	100	mm
Rear fender gap	g_r	100	mm
Wheel diameter	r_t	661	mm
Approach angle	β_f	40	deg
Departure angle	β_r	41	deg
Roll center height	–	215.06	mm

The Suzuki Vitara is equipped with a front MacPherson strut suspension. To characterize the original MacPherson suspension, a reverse engineering procedure was performed. The suspension assembly was partially disassembled from the vehicle to facilitate direct measurements of key components, such as the control arm, shock absorber, and steering knuckle. A 3D scanner (Creality Raptor) was used to capture the geometry of the main structural elements and mounting points. The scanned data and technical specifications were imported into CAD software to create a 3D model of the stock MacPherson suspension and the corresponding chassis mounting points. This model served as a reference to ensure that any new suspension design would fit existing spatial constraints and fastening locations.

A MacPherson suspension can be viewed as an inverted slider mechanism, where the chassis is the ground link and the wheel-carrying link functions as a coupling joint. It typically consists of a shock absorber, a coil spring, and a single lower control arm, all mounted to the chassis. Figure 2 shows the reverse engineering CAD model and a simplified kinematic representation of the stock MacPherson suspension for the Suzuki Vitara and its original dimensions are shown in Table 2.

Table 2. Measurements of the original MacPherson suspension system in nominal position.

Description	Symbol	Value	Unit
Strut length	a	629.34	mm
Control arm length	b	404.41	mm
Chassis link length	c	614	mm
Strut angle	θ_1	36.9	deg
Lower arm angle	θ_2	73.1	deg
Damper length	ℓ_d	485.7	mm
Spring length	ℓ_s	180.79	mm

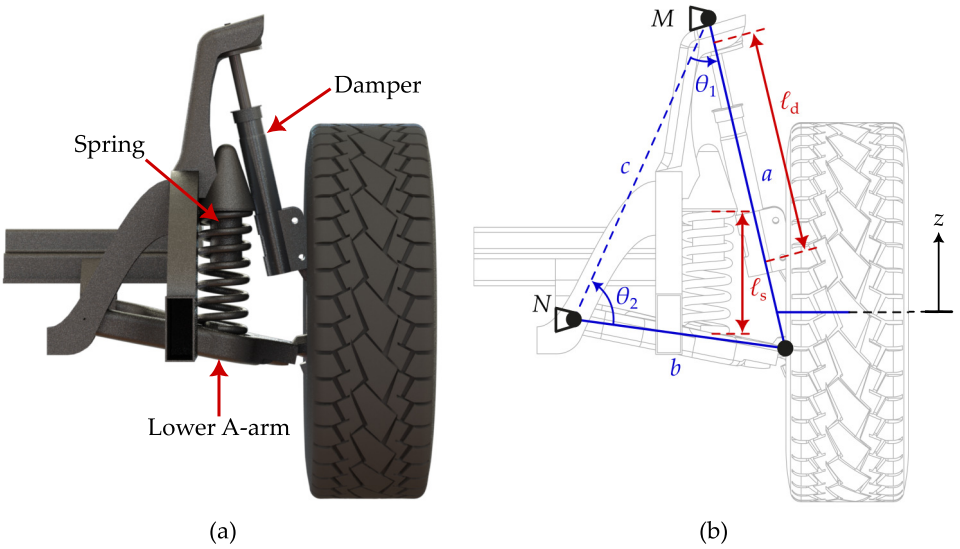

Figure 2. Original MacPherson suspension: (**a**) CAD render obtained via reverse engineering and 3D scanning; (**b**) simplified kinematic model.

A double wishbone, or double A-arm suspension, can be seen as a four-bar mechanism in which the chassis serves as the ground link and the wheel is carried by one of the joints. For this particular vehicle, the coil is positioned between the lower A-arm and the chassis, with the shock absorber attached above the upper A-arm, as illustrated in Figure 3. Alternatively, the spring can be installed between the upper arm and the chassis, or between the upper and lower A-arms. In either configuration, the arm supporting the spring is strengthened, while the other arm acts as a connecting link.

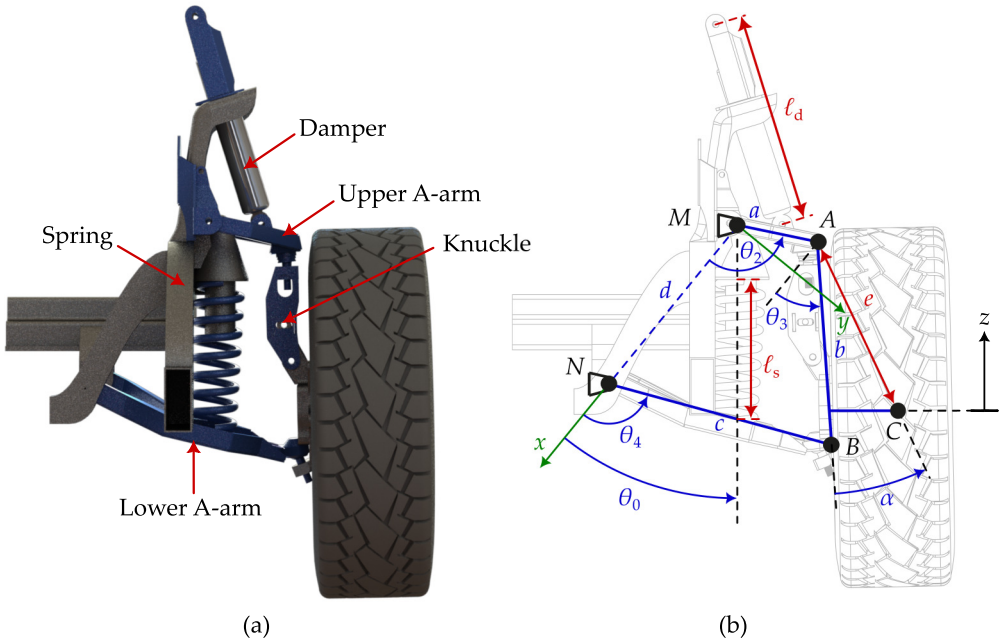

Figure 3. Modified double wishbone suspension: (**a**) CAD render; (**b**) simplified kinematic model.

The kinematic analysis is based on the formulation of Jazar [19]. As shown in Figure 3 the wheel is attached to a coupler point C of the mechanism. A local suspension coordinate frame (x, y) is established, with the x axis indicating the ground link MN, which maintains a constant angle θ_0 relative to the vertical axis. The suspension mechanism has lengths a for the upper A-arm, b for the coupler link, c for the lower A-arm, and d for the ground link. The suspension configuration is determined by the angles θ_2, θ_3, and θ_4, while α

defines the orientation of the distance AC (length e) with respect to the coupler link. Angle θ_3 denotes the suspension camber, which can be calculated as a function of the vertical displacement z of the point C. The coordinates of point C (x_C, y_C) can be calculated using θ_2 as a parameter:

$$x_C = a\cos\theta_2 + e\cos\delta \tag{1}$$

$$y_C = a\sin\theta_2 + e\sin\delta \tag{2}$$

where

$$\delta = \tan^{-1}\left(\frac{a\sin\theta_2}{d - a\cos\theta_2}\right) - \tan^{-1}\left(\frac{\sqrt{4b^2f^2 - [b^2 + f^2 - c^2]^2}}{b^2 + f^2 - c^2}\right) + \alpha \tag{3}$$

$$f = \sqrt{a^2 + d^2 - 2ad\cos\theta_2} \tag{4}$$

The position of the coupler point is defined as

$$\mathbf{u}_C = x_C\hat{i} + y_C\hat{j} \tag{5}$$

and hence, the vertical displacement is given by

$$z = \mathbf{u}_C \cdot \hat{u}_z = -x_C\cos\theta_0 - y_C\sin\theta_0 \tag{6}$$

with

$$\hat{u}_z = -\cos\theta_0\hat{i} - \sin\theta_0\hat{j} \tag{7}$$

The initial coordinates (x_C^*, y_C^*) can be calculated using Equations (1) and (2). Subsequently, the values obtained can be substituted in Equation (6) to determine z^*. Here, the asterisk subscript denotes the initial positions taken in the nominal position of the vehicle. The vertical displacement of the wheel center is $\Delta z = z - z^*$. The initial angle of the link of the coupler in the vertical direction is $\theta_0 - \theta_3^*$. Therefore, the camber angle of the wheel is governed by

$$\gamma = (\theta_0 - \theta_3) - (\theta_0 - \theta_3^*) = \theta_3^* - \theta_3 \tag{8}$$

The angle of the coupler link with respect to the x axis is

$$\theta_3 = 2\tan^{-1}\left(\frac{\sin\theta_2 \pm \sqrt{\sin^2\theta_2 - [J_5 - J_1 + (1 + J_4)\cos\theta_2][J_5 + J_1 - (1 - J_4)\cos\theta_2]}}{J_5 - J_1 + (1 + J_4)\cos\theta_2}\right) \tag{9}$$

where

$$J_1 = d/a \tag{10}$$

$$J_2 = d/c \tag{11}$$

$$J_3 = \frac{a^2 - b^2 + c^2 + d^2}{2ac} \tag{12}$$

$$J_4 = d/b \tag{13}$$

$$J_5 = \frac{c^2 - d^2 - a^2 - b^2}{2ab} \tag{14}$$

Equation (8) can be used to determine the behavior of the camber angle with the help of Equations (6) and (9). Thus, γ can be expressed as a function of z to provide information on how parametric variations in the length of the suspension arm affect the vehicle's kinematic behavior.

The original lower A-arm measures approximately 404 mm. The range chosen for the lower A-arm, from 396 mm to 446 mm, was designed to allow systematic exploration of suspension kinematics while ensuring that the front and rear track widths remain consistent. Similarly, the upper length of the A-arm varies from 142 mm to 192 mm. These ranges were determined by analyzing the available space within the chassis using the CAD model, ensuring that the new arms would fit within the existing design and without interfering with other components.

2.1. Camber Angle Analysis

A reduced variation of camber angle ensures that the surface of the tire maintains maximum contact with the ground during cornering. In addition, a negative camber, where the top of the tire is closer to the vehicle than the bottom, can potentially improve grip in turns. Figure 4 shows a sensitivity analysis of the variation in camber angle (γ) as a function of wheel travel for the proposed double wishbone suspension. Each curve represents a different combination of upper and lower arm lengths, color-coded and labeled in the legend. In general, the camber angle behavior is nonlinear and concave. At equilibrium, the wheel is set to 0 deg camber; however, as the suspension extends slightly, a slight positive incline is induced due to the specific orientation and length of the upper arm. As the height increases further, geometric constraints force the camber to transition back to a negative value. This is a design feature that improves lateral grip during cornering by optimizing the tire contact patch under higher loads [20]. Moreover, variations in the upper arm's length alter the sensitivity of the camber response. A shorter upper arm produces a more abrupt change, while a longer arm produces a smoother transition [21]. The dashed black curve in Figure 4 represents the selected configuration, which finds a trade-off between the variation in camber angle and mechanical constraints in the suspension envelope ($a = 167$ mm, $c = 421$ mm).

Given that this vehicle is designed for off-road conditions, maintaining equal track widths on both axles is essential to ensure balanced load distribution, stable handling in curves, and consistent traction between the axles. After this selection, the details of the final dimensions of the proposed double wishbone suspension are presented in Table 3. The remainder of the analysis and prototype construction is developed on the basis of the obtained results.

Table 3. Dimensions of the final design for the double wishbone suspension system in nominal position.

Description	Symbol	Value	Unit
Strut length	a	167	mm
Control arm length	b	362.7	mm
Chassis link length	c	421	mm
Ground link length	d	388.3	mm
Distance from A to C	e	326.8	mm
Damper length	ℓ_d	413	mm
Spring length	ℓ_s	244	mm
Ground link orientation angle	θ_0	36.95	deg
Upper arm angle	θ_2	102.8	deg
Coupler angle	θ_3	39.8	deg
Lower arm angle	θ_4	110	deg
Coupler angle	α	22.5	deg

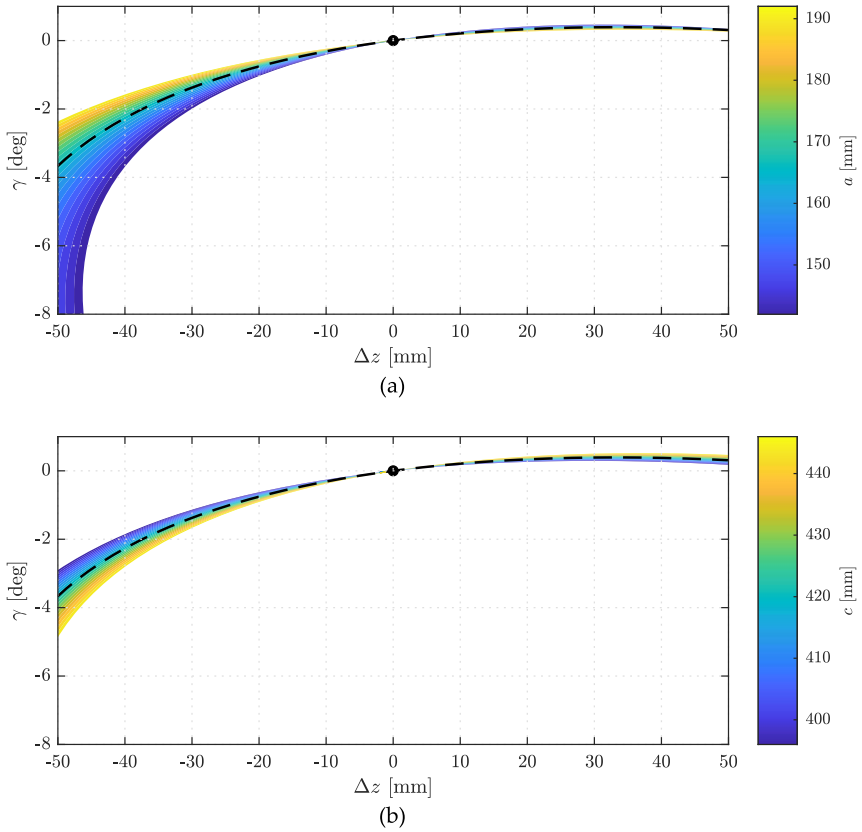

Figure 4. Variation of the angle gamma as a function of the wheel vertical displacement for different lower and upper arm lengths in the double wishbone suspension configuration. Plot (**a**): $a = 142$–196 mm, $c = 421$ mm. Plot (**b**): $a = 167$ mm, $c = 396$–446 mm.

2.2. Caster Angle Analysis

Caster λ is the angle measured between the steering axis and the vertical axis from a side view. In most cases, positive λ improves steering wheel return capabilities by introducing a higher self-aligning torque, thus improving straight-line driving [22]. As shown in Figure 5, the caster angle (λ) for the original MacPherson strut suspension system is 2 deg, while the modified double wishbone suspension system increases λ to 3.1 deg.

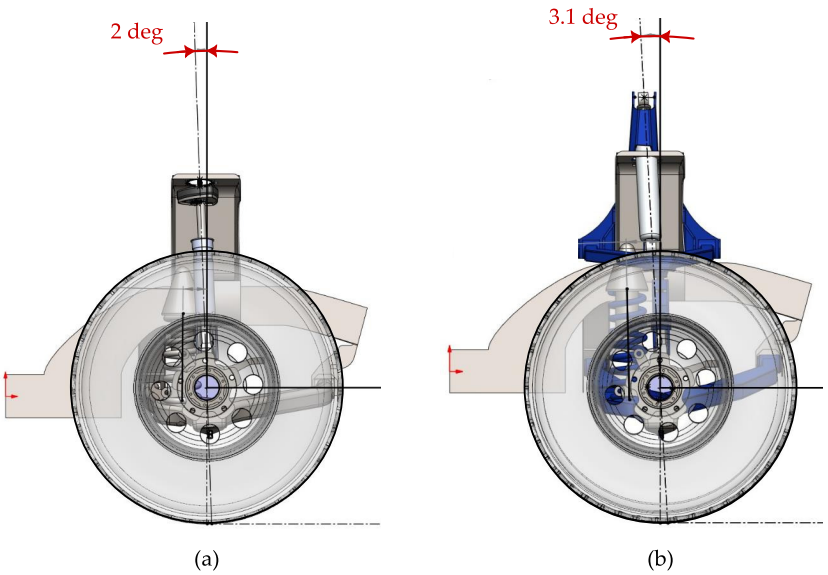

Figure 5. Caster angle in function of the vertical line. (**a**) original MacPherson suspension, and (**b**) modified double wishbone suspension.

2.3. Motion Ratio Analysis

The motion ratio is defined as the ratio between the wheel displacement (Δz) and the stroke of the shock absorber (ℓ_d) or the spring (ℓ_s). Since the spring and the damper are not coaxial in both the original and the proposed suspensions, motion ratios for each case should be defined. The comparison of the motion ratios for the original and modified suspension systems is presented in Figure 6.

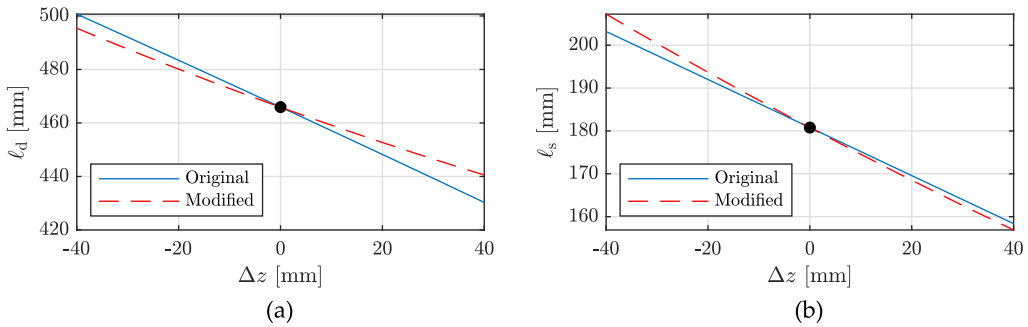

Figure 6. Comparison of motion ratios for suspension components: (**a**) damper and (**b**) spring.

The motion ratios can be quantified with the information in Figure 6, specifically by obtaining the derivative of each curve at the nominal position $\Delta z = 0$. The curves obtained through kinematic analysis show a linear behavior, which yields a coefficient of determination $R^2 > 0.98$ when approximated with a first degree polynomial. In particular, the motion ratio of the damper decreases from 0.88 to 0.68. A lower motion ratio allows for a shorter damper stroke, thus reducing the probability of hitting the bump stop when traveling through uneven terrain. This represents a crucial advantage for small vehicles 4×4, as reaching the end of the stroke usually induces discomfort among passengers. In contrast, the spring motion ratio increases from 0.56 to 0.63. However, in this case, the element that limits the suspension stroke is the damper. Taking into account the differences in motion ratios, the stiffness and damping parameters must be adapted to match a similar response for both suspension configurations. These aspects will be covered in the following section.

2.4. Vertical Dynamics

To assess the dynamic behavior of the vehicle with both suspensions, the quarter car model depicted in Figure 7 is used. In this model, the vehicle chassis is represented as one quarter of its total mass to define the sprung mass: $m_s = 412\,\text{kg}$. The unsprung mass $m_u = 55\,\text{kg}$ represents the wheel hub assembly, connected to the road by means of the stiffness of the tire $k_t = 313\,\text{kN/m}$. Both bodies are connected through the suspension, with stiffness k_{eq} and viscous damping coefficient c_{eq}. These equivalent parameters are obtained from the following relationship for both the MacPherson and double wishbone architectures:

$$x_{eq} = \mu^2 x_c \tag{15}$$

where x denotes the parameter of interest, stiffness or damping, and α is the generic motion ratio. The subscripts eq and s indicate the quarter car or component level, respectively.

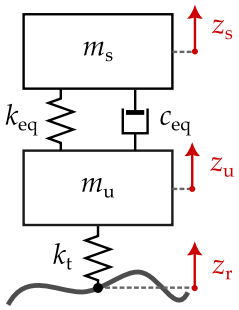

Figure 7. Quarter car model to represent vertical dynamics for both suspension systems.

With the aid of Equation (15), Table 4 is populated with the suspension parameters at the levels of the components and quarter car. The natural frequency of the sprung mass can be approximated through

$$f_s = \frac{1}{2\pi}\sqrt{\frac{k_{eq}}{m_s}} \tag{16}$$

The proposed double wishbone configuration slightly increases the natural frequency of the chassis from 1.12 to 1.29 Hz; however, this new value is well within the limits of an automobile suspension. Furthermore, the damping coefficient is slightly increased to provide better road holding at the cost of decreased passenger comfort. This tradeoff is well known in suspension systems [22] and can be tuned according to application preferences.

Table 4. Suspension parameters at the component and quarter car levels.

Suspension	Parameter	Value	Unit
MacPherson	Suspension stiffness	65	kN/m
	Spring motion ratio	0.56	–
	Quarter car eq. stiffness	20.4	kN/m
	Sprung mass natural frequency	1.12	Hz
	Suspension damping	4	kNs/m
	Damper motion ratio	0.88	–
	Quarter car eq. damping	3.03	kNs/m
Double wishbone	Suspension stiffness	70	kN/m
	Spring motion ratio	0.63	–
	Quarter car eq. stiffness	26.9	kN/m
	Sprung mass natural frequency	1.29	Hz
	Suspension damping	9	kNs/m
	Damper motion ratio	0.68	–
	Quarter car eq. damping	4.16	kNs/m

The proposed quarter car is governed by a set of two ordinary differential equations:

$$m_s\ddot{z}_s + c_{eq}(\dot{z}_s - \dot{z}_u) + k_{eq}(z_s - z_u) = 0 \tag{17}$$

$$m_u\ddot{z}_u + c_{eq}(\dot{z}_u - \dot{z}_s) + k_{eq}(z_u - z_s) + k_t(z_u - z_r) = 0 \tag{18}$$

where z_s, z_u denote the degrees of freedom of the sprung and unsprung masses, respectively. The displacement z_r describes the perturbation of the road profile.

2.4.1. Frequency Domain Anawlysis

Equations (17) and (18) can be transformed into the frequency domain (complex variable s) to calculate two transfer functions of interest:

$$G_{\mathrm{a}}(s) = s^2 \frac{z_{\mathrm{s}}(s)}{z_{\mathrm{r}}(s)} \tag{19}$$

$$G_{\eta}(s) = \frac{k_{\mathrm{t}}}{(m_{\mathrm{s}} + m_{\mathrm{u}})g} \frac{z_{\mathrm{u}}(s) - z_{\mathrm{r}}(s)}{z_{\mathrm{r}}(s)} \tag{20}$$

Equation (19) represents the response of the vehicle chassis acceleration as a function of the input of the road profile. Its value is directly related to passenger comfort, according to the ISO 2631 standard [23]. In contrast, Equation (20) describes the behavior of the so-called road holding index as a function of the road profile input. This dimensionless quantity is the ratio between the elastic force of the tire and the weight of the vehicle, calculated as the product of the total mass and the gravity acceleration g. The values of the road holding index above the unit indicate that the tire elongation force has overcome the weight of the vehicle, thereby implying the detachment of the tire from the ground. The road holding index is a safety metric; constant contact with the ground is key to ensure proper traction and vehicle overall stability. The magnitude frequency responses for the two transfer functions described above are plotted in Figure 8. The selection of a larger damping coefficient for the modified suspension (double wishbone) is observed to produce lower values of the road holding index above 8 Hz, including the resonance of the wheel hub assembly (∼13 Hz). This choice comes at the cost of increasing the magnitude of the sprung mass acceleration across all the analyzed frequency spectrum. Nevertheless, in off-road conditions, road-holding safety is preferred over passenger comfort.

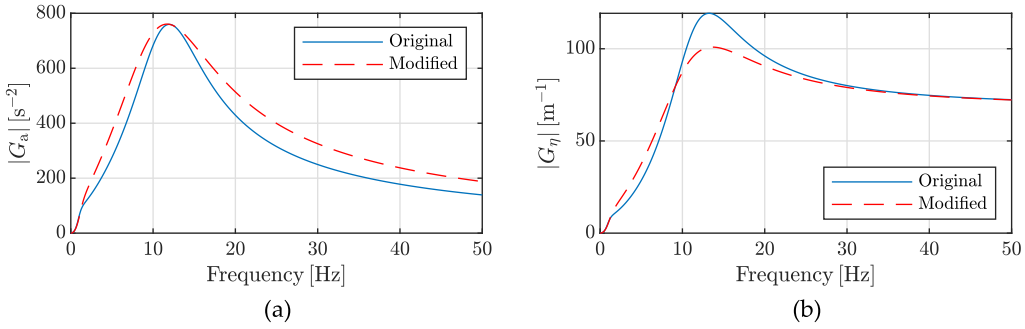

Figure 8. Magnitude frequency response functions for (**a**) $G_{\mathrm{a}}(s)$ for sprung mass acceleration, and (**b**) $G_{\eta}(s)$ for road holding index.

2.4.2. Time Domain Analysis

Equations (17) and (18) can be numerically integrated for a given input profile $z_{\mathrm{r}}(t)$ in the time domain. To this end, the a road profile was synthesized for an ISO class D condition and a vehicle travel speed of 20 km/h [24]. Furthermore, to account for the human comfort perception, a weighting filter was applied to the sprung mass acceleration, according to the ISO 2631 standard [24]. Acceleration and road holding root-mean-square (RMS) metrics were extracted for both suspension configurations. The MacPherson configuration led to an RMS weighted acceleration of 1.6 m/s^2, whilst the double wishbone counterpart yielded a worse performance, as expected: 1.88 m/s^2. The RMS value of the road holding index was 0.27 for both suspensions.

To obtain a more detailed insight on the transient performance of the systems under test, a speed bump test was fed as the input profile. Considering a vehicle speed of 20 km/h, a half-sinusoidal obstacle with a height of 50 mm and a width of 400 mm was fed to the

time domain model. Due to the fast transient nature of the test, an equivalent length must be considered to model the contact between the tire and the ground. In this case, a constant length of 80 mm represents this region. The end portions of the wheel are used to average the road profile. Figure 9 shows the results of the speed bump test in terms of weighted acceleration and road holding index. Suspension responses are overlapped to give means of comparison.

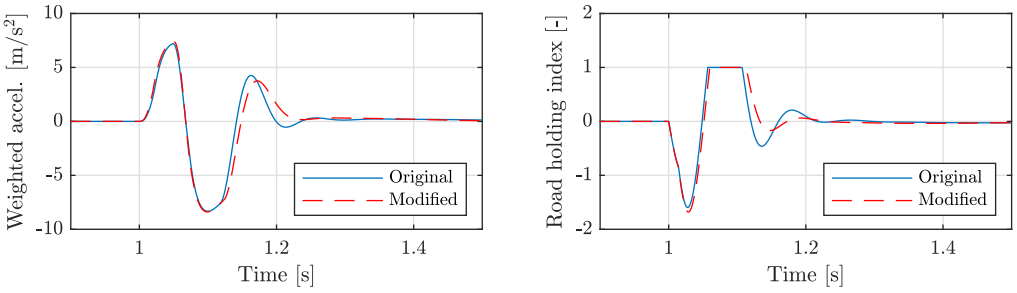

Figure 9. Bump response in the time domain for (**a**) sprung mass weighted acceleration, and (**b**) road holding index.

Both suspensions give comparable results in the first phase of the response, where peaks are reached for the weighted acceleration and the road holding index. For the latter, the tire force was limited in the model to simulate the detachment of the wheel. This phenomenon is observed between 1.06 and 1.11 s in both suspension cases. However, it is seen that the modified suspension (double wishbone) reacts faster for the rest of the transient, leading to a slightly more damped response and a consequently reduced settling time.

3. Implementation

The proposed double wishbone suspension was installed in the target vehicle. Figure 10 shows a picture that compares both the original MacPherson suspension and the modified double wishbone suspension.

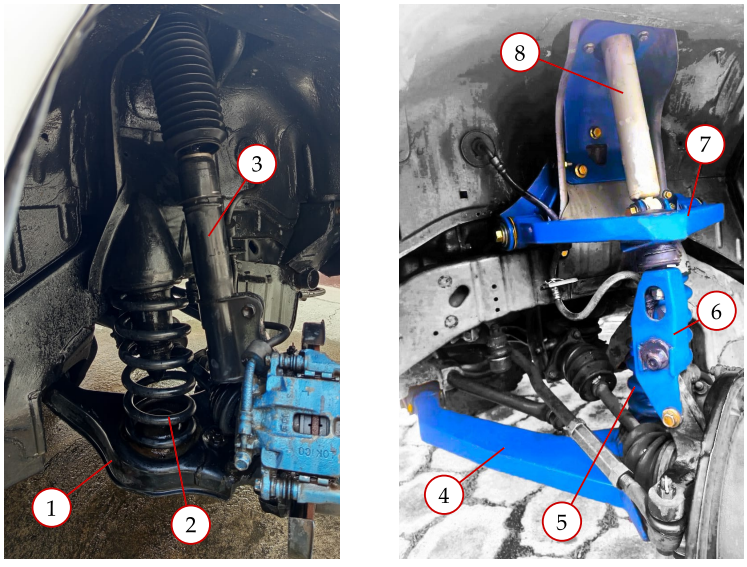

Figure 10. Vehicle with front suspension installed: (**a**) original MacPherson suspension with (1) lower A-arm, (2) spring, (3) damper; (**b**) modified double wishbone suspension with (4) lower A-arm, (5) spring, (6) knuckle, (7) upper A-arm, (8) damper.

This implementation led to the final geometric parameters of the vehicle listed in Table 5, where the original and modified characteristics are referred to the geometry in Figure 1. One of the most significant modifications is the ground clearance h_g. Increasing the ground clearance raises the vehicle's overall height, improving its capacity and enabling it to overcome obstacles with ease. Furthermore, a larger approach β_f and departure β_r allow the vehicle to tackle obstacles with steeper ramps or inclines without making contact with the ground during ascent or descent, respectively. In fact, larger approaches and departure angles significantly improve safety in off-road vehicles by making it easier to overcome various obstacles, improving traction and stability, and providing greater comfort when navigating challenging terrain.

Table 5. Dimensions of the vehicle before and after modifications.

Description	Symbol	Original	Modified	Unit
Track width	w_t	1395	1500	mm
Ride height	h_t	220	333	mm
Overall height	h_t	1665	1800	mm
Wheelbase	ℓ_b	2200	2200	mm
Ground clearance	h_g	240	360	mm
Front fender gap	g_f	100	230	mm
Rear fender gap	g_r	100	240	mm
Wheel diameter	r_t	661	762	mm
Approach angle	β_f	40	58	deg
Departure angle	β_r	41	56	deg
Roll center height	–	215.06	315.97	mm

According to Table 5, the roll center increased about 100 mm. The higher the roll center, the shorter the lever arm between the center of gravity and the roll center becomes, resulting in the chassis/body rocking very little inward and outward, better transferring the load to the wishbones and springs that make up the suspension, thereby reducing pitching through better load distribution to the entire suspension system compared to the original.

The increased caster angle from 2.01 deg (MacPherson) to 3.1 deg (double wishbone) improves stability, which is crucial for off-road or high-performance vehicles. Double wishbone suspension with higher caster provides better control on uneven terrain, helping front wheels return to their center position more easily compared to the original system. In curves, the higher caster generates a camber effect, which results in better tire grip and grip in high-speed turns.

Figure 11 presents a comparison of the camber angle behavior as a function of the vertical movement of the wheel, Δz, between the original (MacPherson) and the modified (double wishbone) suspensions. For the MacPherson suspension, the camber angle begins at approximately -1.74 deg at a height of -54 mm, becoming less negative as it approaches the static level (0 mm), where it reaches around -0.06 deg. The angle of camber increases to approximately 2.41 deg at a height of 106 mm. This shift from a negative camber during compression suggests changes in the contact of the tire with the road.

In contrast, the modified suspension exhibits a more gradual variation in camber angle with suspension travel. When the suspension is extended, the camber angle starts at approximately -4.82 deg at -55 mm and gradually increases, reaching -0.05 deg in nominal position. As the suspension compresses, the camber angle becomes positive, peaks at about 0.39 deg at 34 mm before gradually decreasing to around -0.68 deg at 98 mm. Compared to the MacPherson system, the double wishbone suspension appears to maintain more consistent tire contact and stability throughout suspension travel, which could lead to improved ride quality and reduced tire wear [11].

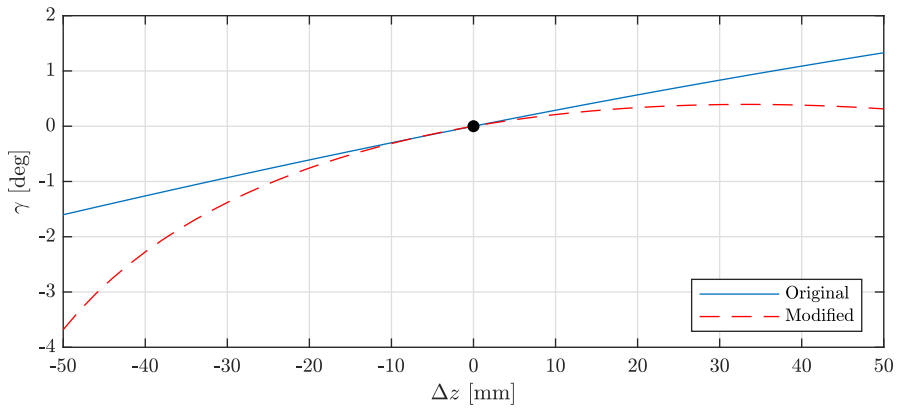

Figure 11. Camber angle as a function of the wheel vertical displacement for the original Macpherson and modified double wishbone suspensions.

3.1. On-Road Test Procedure

Experimental testing was conducted on the ICE-powered Vitara to collect real-world data. A cost-effective data logger was utilized, featuring a Bosch Sensortec BMA400 triaxial accelerometer, to capture vertical, lateral, and longitudinal acceleration components during test drives. The device was mounted in the driver's corner to ensure a practical and consistent installation. This setup was replicated for both the original MacPherson strut suspension and the proposed double wishbone configuration tests. Data were collected at a sampling frequency of 100 Hz. This acquisition rate was considered sufficient to capture chassis dynamics, whose resonant frequency usually falls between 1.1 and 1.5 Hz.

Both suspension setups were tested under comparable speeds and load conditions, with the vehicle traveling along the same route—consisting of urban streets and light off-road sections—to encompass a range of impacts and maneuvers. The acceleration data collected offer information on whether the proposed double wishbone geometry enhances comfort or stability compared to the baseline configuration.

The test was carried out on a closed circuit in the city of Ibarra, Ecuador, on a dirt terrain characterized by an irregular surface composed of soil and stones, as shown in Figure 12. This route was specifically selected to allow low-speed testing and ensure repeatability of measurements for both vehicle configurations. The circuit presents an altitude variation of 27.6 m, with a maximum altitude of approximately 2158.6 m above sea level. It has a total travel distance of 625.65 m. The moderate change in altitude and the type of terrain in the circuit are representative of the typical topography of the region.

The circuit did not include any artificial obstacles beyond the natural irregularities of the surface. Starting and ending at the same point, the route comprised a straight section from the start to the point (1), a sharp turn at the point (1), another straight segment from the point (1) to the point (2), a wide turn between the points (2) and (3), and a final straight path from point (3) back to the endpoint.

During the test, an average speed of 2.51 m/s was registered; the maximum speed recorded was 5.28 m/s. In the sharper 90 deg right turn, the average speed was 3.24 m/s; and in the wider curve, the speed reached was 4.61 m/s.

Figure 12. Route in Ibarra, Ecuador, used to compare vehicles fitted with original and modified suspensions under the same test conditions. Satellite image downloaded using Google Earth. Straight section followed by a sharp turn in (1), wide turn between points (2) and (3).

3.2. On-Road Test Results

Key metrics, such as mean, standard deviation, minimum, and maximum values, are used to quantify the response of each suspension to dynamic forces under various driving conditions. This analysis aims to identify which suspension offers better stability, comfort, and control, highlighting areas where the modified system improves or falls short compared to the original. Table 6 presents the mean and standard deviation of the acceleration components along the x, y and z axes of the vehicle reference frame, as defined in Figure 1.

Table 6. Accelerations data for both suspension configurations.

Axis	Mean [m/s^2]		Std. Dev. [m/s^2]	
	Original	Modified	Original	Modified
x	0.56	0.0016	1.45	2.71
y	1.23	1.23	1.7	1.74
z	9.59	9.61	3.06	4.49

3.2.1. Lateral Acceleration Forces

The modified suspension system shows higher variability in lateral acceleration compared to the original MacPherson strut design. In the context of off-road driving, this characteristic reflects improved wheel articulation and greater responsiveness to abrupt terrain changes. Additionally, the increased lateral acceleration is consistent with the higher center of mass introduced by the modified setup, which naturally results in a more pronounced vehicle roll when traveling on uneven surfaces. The modified suspension supports wider extreme values (minimum and maximum), related to a larger dynamic range; see Figure 13 and Table 7.

Table 7. Lateral acceleration values for both suspension configurations in sharp and wide turns.

Track Point	Time [s]	Mean [m/s^2]		Std. Dev. [m/s^2]	
		Original	Modified	Original	Modified
Sharp turn	39	0.25	0.16	1.5	1.93
Wide turn	139	0.47	0.16	1.64	3.1

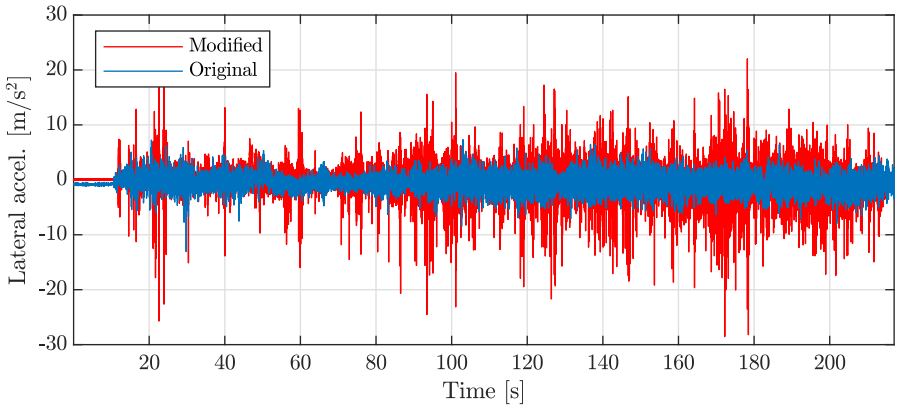

Figure 13. Lateral acceleration for both suspension configurations along the test track.

The modified suspension consistently shows a lower mean lateral acceleration (0.16 m/s^2) in both the sharp and wide turn sections compared to the original MacPherson setup (0.25 m/s^2 and 0.47 m/s^2, respectively). This indicates that on average, the modified suspension leads to less steady-state lateral load at these track points, potentially due to more compliant or better-articulated wheel motion, especially useful in off-road conditions where terrain irregularities are prevalent. In contrast, the standard deviation of the lateral acceleration is higher in the modified suspension, particularly in the wide turn (3.10 m/s^2 and 1.64 m/s^2 respectively). This reflects greater fluctuation, suggesting that the double wishbone setup is more responsive and reacts more dynamically to uneven terrain, resulting in more pronounced movements of the vehicle body. The higher standard deviation suggests that the modified suspension is more sensitive to disturbances and terrain variations, which is beneficial in off-road conditions, where fast response and flexibility in wheel movement are crucial.

3.2.2. Longitudinal Acceleration Forces

Comparison of longitudinal acceleration between original MacPherson and modified double wishbone suspension highlights distinct differences in dynamic behavior, as shown in Figure 14. At the sharp turn (39 s), the mean longitudinal acceleration increases from 0.03 m/s^2 (original) to 0.13 m/s^2 (modified), as reported in Table 8. The standard deviation also rises slightly, from 1.11 m/s^2 to 1.16 m/s^2, suggesting marginally more fluctuation, but within a comparable range. During the wide turn (139 s), both configurations exhibit similar mean values (1.91 m/s^2 for the original configuration and 1.90 m/s^2 for the modified one), but the standard deviation decreases noticeably with the modified suspension, from 1.87 m/s^2 to 1.56 m/s^2, reflecting improved stability and smoother longitudinal behavior. These trends are consistent with the data in Table 8: in the sharp turn segment, the modified setup maintains a slightly higher mean value -0.03 m/s^2 for the original, 0.13 m/s^2 for the modified one) and standard deviation (1.16 m/s^2 for the original one, 1.11 m/s^2 for the modified one), while in the wide turn, it shows nearly identical mean values (1.90 m/s^2 and 1.91 m/s^2 for the original and modified one respectively) but a lower standard deviation (1.56 m/s^2 and 1.87 m/s^2). This reduction in variability, especially in the wider turn, suggests that the modified suspension provides a more consistent and predictable response to terrain input. This aspect is beneficial, especially for off-road driving, where traction management and vehicle balance are critical. Regarding the minimum and maximum longitudinal acceleration values, the original suspension ranged between -4.03 m/s^2 and 3.37 m/s^2, while the modified suspension had slightly narrower variations, ranging between -3.83 m/s^2 and 3.73 m/s^2.

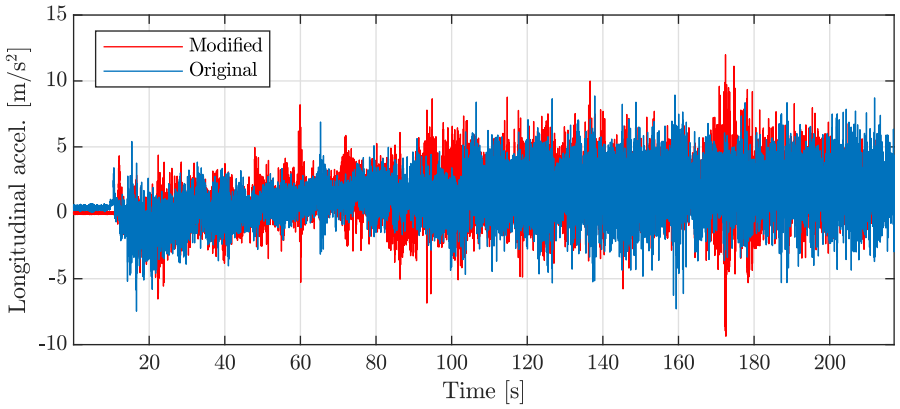

Figure 14. Longitudinal acceleration forces and course route.

Table 8. Longitudinal acceleration values for both suspension configurations in sharp and wide turns.

Route		Mean	Std. Dev.	Min.	Max.
Sharp Turn (39 s)	Original	−0.03	1.11	−4.02	3.36
	Modified	0.13	1.16	−3.82	3.72
Wide Turn (139–166 s)	Original	1.91	1.87	−7.28	8.93
	Modified	1.90	1.56	−5.28	7.81

3.2.3. Vertical Acceleration Forces

The comparison of vertical acceleration between the original MacPherson and modified double wishbone suspension configurations shown in Figure 15 reveals that both setups experience similar average vertical loads, but with notable differences in variability. At the sharp turn (39 s) in Table 9, the mean vertical acceleration is nearly identical between the two configurations, with 9.72 m/s^2 for the original and 9.79 m/s^2 for the modified. However, the standard deviation increases significantly from 2.2 m/s^2 (original) to 3.43 m/s^2 (modified), indicating that the modified suspension experiences more vertical oscillations during the experimental test performed. A similar trend is observed in the wide turn (139 s) in Table 9, where the mean values are similar (9.55 m/s^2 for MacPherson and 9.53 m/s^2 for double wishbone suspension) while the standard deviation increases substantially, from 3.76 m/s^2 to 5.08 m/s^2. These results suggest that although the average vertical load remains consistent across both suspension archetypes, the modified suspension transmits more pronounced vertical dynamics to the vehicle body, which is mainly attributable to the increased vehicle height due to the installation of the double wishbone suspension.

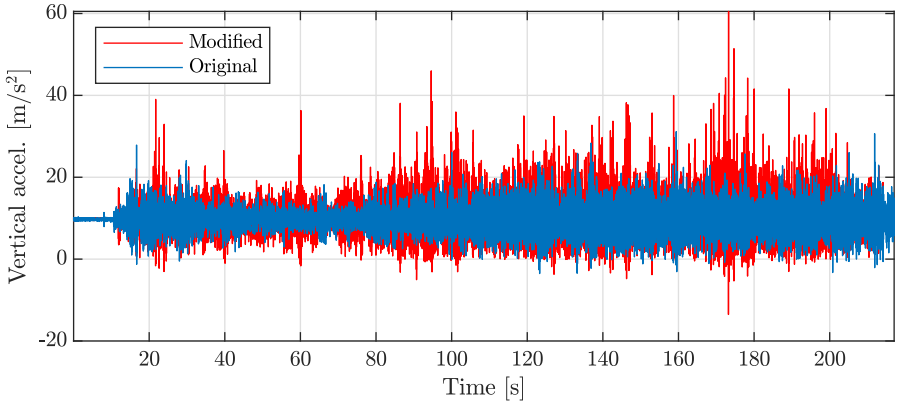

Figure 15. Vertical acceleration forces and course route.

Table 9. Data comparison in sharp and wide turn vertical accelerations z-axis.

Track Point	Time [s]	Mean [m/s^2]		Std. Dev. [m/s^2]	
		Original	Modified	Original	Modified
Sharp turn	39	9.72	9.79	2.2	3.43
Wide turn	139	9.55	9.53	3.76	5.08

4. Conclusions

This study demonstrates the relevance of optimizing suspension configurations in electric off-road vehicles, particularly the transition from a MacPherson strut system to a double A-arm architecture. The proposed suspension showed significant improvements in dynamic behavior, especially in terms of camber angle control throughout the entire wheel travel range. The improved control allowed for more consistent contact of the tire with the ground, contributing to better grip during cornering, reduced tire wear, and increased predictability of vehicle handling in challenging driving conditions.

Kinematic and dynamic analysis revealed that the double wishbone system improves road-holding performance at higher frequencies, although it induces slightly higher vertical accelerations, as indicated by increased RMS values. This trade-off, while marginally reducing passenger comfort, is acceptable in off-road scenarios, where vehicle safety and tire-road contact are prioritized. Time-domain analysis further confirmed that the modified suspension reacts faster and settles more rapidly after transient events such as bumps, thus enhancing overall ride stability.

Additionally, the redesign yielded substantial increases in ground clearance, approach and departure angles, and roll center height, all of which are critical for off-road applications. These geometric modifications allow the vehicle to traverse uneven terrain more effectively and offer better protection for underfloor battery packs. Despite a higher center of gravity, the elevated roll center helps redistribute loads more efficiently across the suspension components, reducing chassis roll and improving stability during cornering.

Real-world on-road tests conducted under off-road conditions confirmed the findings obtained by simulation. The modified suspension exhibited greater variability in lateral and vertical acceleration, reflecting its enhanced responsiveness and adaptability to terrain irregularities. At the same time, lower mean lateral acceleration values during sharp and wide turns indicated smoother wheel articulation, a beneficial characteristic for off-road driving.

The findings in this work demonstrate the versatility of specific vehicle platforms, where the chassis can be adapted to different suspension layouts. For car makers, this represents a potential increase in their product portfolio, as solutions can be adapted according to the use scenario (e.g., urban or off-road). This also opens the possibility of platform conversion towards electrification.

Future research could explore adaptive suspension systems that dynamically regulate camber based on real-time driving conditions, potentially incorporating an additional shock absorber for greater oscillation control. Furthermore, experiments are planned with an actual electric-converted version of this vehicle model, equipped with a custom battery pack mounted on the vehicle floor. Such efforts will provide direct insight into how the redesigned suspension performs under true electric vehicle operating conditions, further contributing to both robustness and efficiency in off-road environments.

Author Contributions: Conceptualization, P.T., E.T., R.G. and D.S.P.-B.; methodology, P.T., E.T., R.G. and D.S.P.-B.; software, P.T. and E.T. and D.S.P.-B.; validation, V.D.Z.-L., J.C.J.-M. and E.A.L.-C.; formal analysis, P.T., E.T., R.G. and D.S.P.-B.; investigation, P.T. and E.T.; resources, E.A.L.-C.; data curation, P.T. and D.S.P.-B.; writing—original draft preparation, P.T. and D.S.P.-B.; writing—review and editing, E.T. and R.G.; visualization, P.T., E.T., R.G. and D.S.P.-B.; supervision, R.G. and E.A.L.-C.; project administration, R.G. and E.A.L.-C.; funding acquisition, E.A.L.-C. All authors have read and agreed to the published version of the manuscript.

Funding: Pablo Tapia is funded by Tecnologico de Monterrey, Grant No. A01769991, and Consejo Nacional de Humanidades, Ciencias y Tecnologias under the scholarship 1050445. We thank the UISEK University in Ecuador for covering the article processing charges.

Institutional Review Board Statement: Not applicable.

Informed Consent Statement: Not applicable.

Data Availability Statement: The original contributions presented in this study are included in the article. Further inquiries can be directed to the corresponding authors.

Conflicts of Interest: The authors declare no conflict of interest.

Abbreviations

The following abbreviations are used in this manuscript:

AEADE	Asociacion de Empresas Automotrices de Ecuador
AMIA	Asociacion Mexicana de la Industria Automotriz
EV	Electric vehicle
ICE	Internal combustion engine
ISO	International Organization for Standardization
a	Strut length
b	Control arm length
c	Chassis link length
e	Distance from upper arm to coupler
c_{eq}	Quarter car equivalent damping
f_{s}	Sprung mass natural frequency
g	Gravity
g_{f}	Front fender gap
g_{r}	Rear fender gap
h_{g}	Ground clearance
h_{r}	Ride height
h_{t}	Overall height
k_{eq}	Quarter car equivalent stiffness
k_{t}	Tire stiffness
ℓ_d	Damper length
ℓ_{s}	Spring length
m_{s}	Sprung mass
m_{u}	Unsprung mass
r_{t}	Wheel diameter
w_{t}	Track width
$\mathbf{u}_{\mathrm{C}}$	Vector position of point C
x_{c}	Original parameter
x_{eq}	Equivalent parameter
x_{C}	X coordinate of point C

y_C	Y coordinate of point C
z	Vertical displacement
z_s	Sprung mass displacement
z_u	Unsprung mass displacement
z_r	Road profile displacement
G_a	Vehicle chassis acceleration in frequency domain
G_n	Vehicle road holding index in frequency domain
α	Coupler angle
β_f	Approach angle
β_r	Departure angle
γ	Camber angle
λ	Caster angle
μ	Motion ratio
θ_1	Strut angle
θ_2	Lower arm angle
θ_3	vCoupler angle
θ_4	Lower arm angle
Δ_z	Wheel vertical displacement

References

1. AEADE. Sector Automotor en Cifras. 2024. Available online: https://www.aeade.net/wp-content/uploads/2025/01/12.-Sector-en-Cifras-Resumen-Noviembre.pdf (accessed on 15 December 2024).
2. AMIA. Ventas Internas de Vehículos Ligeros. Available online: https://www.amia.com.mx/ventas-internas-de-vehiculos-ligeros/ (accessed on 15 December 2024).
3. Rivera-González, L.; Bolonio, D.; Mazadiego, L.F.; Naranjo-Silva, S.; Escobar-Segovia, K. Long-Term Forecast of Energy and Fuels Demand Towards a Sustainable Road Transport Sector in Ecuador (2016–2035): A LEAP Model Application. *Sustainability* **2020**, *12*, 472. [CrossRef]
4. Wilken, D.; Oswald, M.; Draheim, P.; Pade, C.; Brand, U.; Vogt, T. Multidimensional assessment of passenger cars: Comparison of electric vehicles with internal combustion engine vehicles. *Procedia CIRP* **2020**, *90*, 291–296. [CrossRef]
5. Silva, J.E.d.; Urbanetz Junior, J. Converting a conventional vehicle into an electric vehicle (EV). *Braz. Arch. Biol. Technol.* **2019**, *62*, e19190007. [CrossRef]
6. Lukoševičius, V.; Makaras, R.; Rutka, A.; Keršys, R.; Dargužis, A.; Skvireckas, R. Investigation of vehicle stability with consideration of suspension performance. *Appl. Sci.* **2021**, *11*, 9778. [CrossRef]
7. Triananda, M.; Sumarsono, D.A.; Zainuri, F.; Falah, F.A.; Arrafi, F.; Fauzan, G. Analysis of effect of center of gravity change towards type M1 vehicle stability. *AIP Conf. Proc.* **2021**, *2376*, 070013.
8. Prastiyo, W.; Fiebig, W. Multibody simulation and statistical comparison of the linear and progressive rate double wishbone suspension dynamical behavior. *Simul. Model. Pract. Theory* **2021**, *108*, 102273. [CrossRef]
9. Uberti, S.; Gadola, M.; Chindamo, D.; Romano, M.; Galli, F. Design of a double wishbone front suspension for an orchard-vineyard tractor: Kinematic analysis. *J. Terramechanics* **2015**, *57*, 23–39. [CrossRef]
10. Anand, A.; Verma, A.; Dwivedi, V. Design and Analysis of MacPherson Suspension System and Enhanced Suspension Systems. *Int. J. Mech. Des.* **2024**, *10*, 13–26.
11. Reddy, K.V.; Kodati, M.; Chatra, K.; Bandyopadhyay, S. A comprehensive kinematic analysis of the double wishbone and MacPherson strut suspension systems. *Mech. Mach. Theory* **2016**, *105*, 441–470. [CrossRef]
12. Khan, S.; Joshi, Y.; Kumar, A.; Vemuluri, R.B. Comparative study between double wish-bone and macpherson suspension system. *IOP Conf. Ser. Mater. Sci. Eng.* **2017**, *263*, 062079. [CrossRef]
13. Wang, Y.; Zhao, W.; Zhou, G.; Gao, Q.; Wang, C. Suspension mechanical performance and vehicle ride comfort applying a novel jounce bumper based on negative Poisson's ratio structure. *Adv. Eng. Softw.* **2018**, *122*, 1–12. [CrossRef]
14. Marotta, R.; Strano, S.; Terzo, M.; Tordela, C.; Ivanov, V. *Active Control of Camber and Toe Angles to Improve Vehicle Ride Comfort*; SAE Technical Paper 2022-01-0920; SAE International: Warrendale, PA, USA, 2022; ISSN 0148-7191/2688-3627. [CrossRef]
15. Kavitha, C.; Shankar, S.A.; Karthika, K.; Ashok, B.; Ashok, S.D. Active camber and toe control strategy for the double wishbone suspension system. *J. King Saud Univ.-Eng. Sci.* **2019**, *31*, 375–384. [CrossRef]
16. Audi. The Secret to a Smoother Ride: Electric Vehicle Suspension Explained. Available online: https://www.evsuspension.com/audi/secret-smoother-ride-electric-vehicle-suspension-explained (accessed on 11 August 2024).

17. *ISO 8608:2016*; Mechanical Vibration—Road Surface Profiles—Reporting of Measured Data. International Organization for Standardization: Geneva, Switzerland, 2016.
18. Aneto; Etai. Santana y Suzuki "Vitara". *Rev. Tec. Del Automov.* **1994**, *17*, 72.
19. Jazar, R.N. *Vehicle Dynamics: Theory and Application*; Springer International Publishing: Cham, Switzerland, 2018.
20. Suo, Y.; Yang, W.; Lu, D.; Zhang, Y.; Che, M. Analysis of camber-caused asymmetric characteristics using finite element method and pure camber semi-empirical modeling. *Proc. Inst. Mech. Eng. Part D J. Automob. Eng.* **2024**, 09544070241272802,
21. Park, S.J.; Sohn, J.H. Effects of camber angle control of front suspension on vehicle dynamic behaviors. *J. Mech. Sci. Technol.* **2012**, *26*, 307–313. [CrossRef]
22. Genta, G.; Morello, L. *The Automotive Chassis: Volume 2: System Design*; Springer Nature: Berlin/Heidelberg, Germany, 2019.
23. *ISO 2631-1:1997*; Mechanical Vibration and Shock—Evaluation of Human Exposure to Whole-Body Vibration—Part 1: General Requirements. International Organization for Standardization: Geneva, Switzerland, 1997.
24. Zuo, L.; Zhang, P.S. Energy harvesting, ride comfort, and road handling of regenerative vehicle suspensions. *J. Vib. Acoust.* **2013**, *135*, 1–8. [CrossRef]